Texture-induced spin-orbit coupling and skyrmion-electron bound states in a Néel antiferromagnet

N. Davier [*] and R. Ramazashvili [†]

Laboratoire de Physique Théorique, Université de Toulouse, CNRS, UPS, France

We derive an effective-mass electron Hamiltonian for a Néel antiferromagnet in the presence of a smooth texture of the staggered magnetization. For certain locations of electron band extrema, the texture produces a peculiar and anomalously strong spin-orbit coupling of the scale $\hbar v/L$, with v the Fermi velocity and L the characteristic length scale of the texture. For a skyrmion texture, this coupling generates electron bound states, whose energy scale is given by the gap Δ in the electron spectrum. With dopant carriers, such bound states turn the skyrmion into a charged particle, that can be manipulated by electric field.

I. INTRODUCTION

Topological textures such as domain walls, vortices and skyrmions appear prominently in diverse areas of physics, from cosmology and string theory [1] to QCD, the physics of hadrons, and condensed matter physics [2]. In solid state magnetism alone, topological textures bring together fundamental and applied science, from novel states of matter such as skyrmion crystal to prototype spintronic devices that employ skyrmions and domain walls to process information [3]. While early spintronics research largely focused on ferromagnetic materials [4–6], an ever increasing effort has been turning to antiferromagnets [7,8] and to topological textures therein [9,10]—in view of their technologically attractive properties such as shorter characteristic timescales of the Néel state and its lack of net magnetization [11].

In order to usefully employ topological textures, it is crucial to understand their interplay with other subsystems of a solid, first and foremost—with band electrons. For ferromagnets, much work has been done to understand the influence of a texture on electric current and vice versa [12,13]. Soon after, this effort has been expanded to antiferromagnets [8,14–16].

An important step in this direction has been undertaken by R. Cheng and Q. Niu [17], who studied electron motion in the presence of a texture in a Néel antiferromagnet, using coupled quasiclassical equations of motion for the electron momentum, coordinate and spin. Here we address the same problem fully quantum-mechanically, by deriving the effective-mass Hamiltonian—and show how, for certain locations of electron band extrema, the texture generates a peculiar and anomalously strong spin-orbit coupling, a key result of this work.

It is at this point that we find ourselves following in the footsteps of Solomon Pekar and Emmanuel Rashba [18]. Back in 1964, Pekar and Rashba observed that a nonuniform magnetic field as well as nonuniform magnetization $\mathcal{M}(\mathbf{r})$ give rise to a spin-orbit coupling: exchange interaction $\mathcal{M}(\mathbf{r}) \cdot \boldsymbol{\sigma}$ couples the electron coordinate $\mathbf{r}$ to its spin $\boldsymbol{\sigma}$ via $\mathbf{r}$ dependence of $\mathcal{M}(\mathbf{r})$—that is, simply by virtue of inhomogeneity.

The observation above appears to suggest nondegenerate bands, split by exchange $\mathcal{M}(\mathbf{r}) \cdot \boldsymbol{\sigma}$. Yet symmetry can void this argument by restoring the double degeneracy, as it does for a centrosymmetric Néel antiferromagnet in its uniform state: here, magnetization $\boldsymbol{M}(\mathbf{r})$ changes sign upon translation $\mathbf{T}_a$ by a lattice period a as well as upon time reversal θ. As a result, combined anti-unitary symmetry $I\theta\mathbf{T}_a$, with I the inversion operator, guarantees double degeneracy of Bloch eigenstates throughout the Brillouin zone [19].

A localized texture breaks such a degeneracy-protecting symmetry. Below we illustrate this by a texture in a Néel antiferromagnet, and by an unusual spin-orbit coupling that it produces. Moreover, for a skyrmion texture, this spin-orbit coupling creates electron bound states with energy scale given by the gap Δ in the electron spectrum. With dopant carriers, such bound states turn the skyrmion into a charged particle, another key result of this work.

The paper is organized as follows. In Sec. II, we begin by deriving the low-energy electron Hamiltonian for a centrosymmetric Néel antiferromagnet in the presence of a texture. Then we specify the Hamiltonian for a particular location of the electron band extrema—and point out the appearance of a peculiar spin-orbit coupling. In Sec. III, we present our main example: a texture in the form of a single Belavin-Polyakov skyrmion [20,21]. We show that the texture-induced spin-orbit coupling produces skyrmion-electron bound states, and study their evolution as a function of the skyrmion radius. In Sec. IV, we discuss the implications of our results in the light of the pioneering work [18] of Pekar and Rashba. Finally, Appendices discuss the connection of our results with some of the earlier studies, and outline the validity range of the approximations we used.

II. ELECTRON IN THE PRESENCE OF A TEXTURE

Consider a Néel antiferromagnet on a square-symmetry lattice with period a. In the uniform state, its ordered moment changes sign upon elementary translation, and couples

*davier@irsamc.ups-tlse.fr
†revaz@irsamc.ups-tlse.fr

electron states at any two momenta $\mathbf{p}$ and $\mathbf{p} + \mathbf{Q}$, separated by the Néel wave vector $\mathbf{Q} = (\pm \frac{\pi}{a}, \pm \frac{\pi}{a})$. The coupling has the form of exchange $(\mathbf{\Delta} \cdot \boldsymbol{\sigma})$, with $\mathbf{\Delta}$ proportional to the staggered magnetization, and $\boldsymbol{\sigma}$ the triad of Pauli matrices, representing electron spin. Since $\mathbf{p}$ and $\mathbf{p} + 2\mathbf{Q}$ are equivalent in the Brillouin zone (BZ), the Hamiltonian $\mathcal{H}$ can be written as acting on a bispinor $\Psi = (\psi_{\mathbf{p}}, \psi_{\mathbf{p}+\mathbf{Q}})$ [22]:

$$\mathcal{H} = \begin{bmatrix} \varepsilon(\mathbf{p}) & (\mathbf{\Delta} \cdot \boldsymbol{\sigma}) \\ (\mathbf{\Delta} \cdot \boldsymbol{\sigma}) & \varepsilon(\mathbf{p} + \mathbf{Q}) \end{bmatrix}, \qquad (1)$$

where $\varepsilon(\mathbf{p})$ is the electron dispersion in the absence of Néel order. The spectrum $E_{\mathbf{p}}$ of $\mathcal{H}$ is doubly-degenerate, $E_{\mathbf{p}} = \varepsilon_{+}(\mathbf{p}) \pm \sqrt{|\mathbf{\Delta}|^2 + \varepsilon_{-}^2(\mathbf{p})}$, where $\varepsilon_{\pm}(\mathbf{p}) \equiv \frac{1}{2}[\varepsilon(\mathbf{p}) \pm \varepsilon(\mathbf{p} + \mathbf{Q})]$; it has a gap $\Delta = |\mathbf{\Delta}|$, which turns a half-filled metal into an insulator.

In the presence of a texture $\mathbf{\Delta_r} = \hat{\mathbf{n}}_{\mathbf{r}} \Delta$, unit vector $\hat{\mathbf{n}}_{\mathbf{r}}$ becomes a smooth function of the coordinate $\mathbf{r}$ and carriers near the extrema of $E_{\mathbf{p}}$ at momenta $\mathbf{p}_0$ and $\mathbf{p}_0 + \mathbf{Q}$ admit a low-energy effective-mass description [23]. To derive it, in Eq. (1), we replace uniform $\mathbf{\Delta}$ by $\mathbf{\Delta_r}$, and substitute $\hat{\mathbf{p}} \equiv -i\hbar \boldsymbol{\nabla}$ for the momentum dependences $\varepsilon_{\mathbf{p}_0}(\hat{\mathbf{p}})$ and $\varepsilon_{\mathbf{p}_0+\mathbf{Q}}(\hat{\mathbf{p}})$ of $\varepsilon(\mathbf{p})$ near $\mathbf{p}_0$ and $\mathbf{p}_0 + \mathbf{Q}$.

Now perform a spin rotation $U_{\mathbf{r}}$ that makes $\mathbf{\Delta_r}$ uniform: $U_{\mathbf{r}}^{\dagger}(\hat{\mathbf{n}}_{\mathbf{r}} \cdot \boldsymbol{\sigma})U_{\mathbf{r}} = \sigma_z$ [24]. This generates a Peierls substitution $\hat{p}_i \to \hat{p}_i + (A_i \cdot \boldsymbol{\sigma})$ in $\varepsilon_{\mathbf{p}_0}(\hat{\mathbf{p}})$ and $\varepsilon_{\mathbf{p}_0+\mathbf{Q}}(\hat{\mathbf{p}})$, with $(A_i \cdot \boldsymbol{\sigma}) = A_i^{\alpha} \sigma_{\alpha} = -i\hbar U_{\mathbf{r}}^{\dagger} \partial_i U_{\mathbf{r}}$. Vector potential A_i^{α} carries real-space indices $i = x, y$ and spin indices $\alpha = x, y, z$. While different components of $(A \cdot \boldsymbol{\sigma})$ do not commute, $U_{\mathbf{r}}$ is defined only up to a nonuniform spin rotation $V_{\mathbf{r}}^z = e^{i\sigma_z \chi}$ around $\hat{z}$: $U_{\mathbf{r}} \to U_{\mathbf{r}} V_{\mathbf{r}}^z$, which is an abelian transformation. This gauge transformation acts on $(A \cdot \boldsymbol{\sigma})$ in a peculiar way, elucidated by first-order expansion in infinitesimal χ:

$$\delta(A_i \cdot \boldsymbol{\sigma}) = \hbar \sigma_z \partial_i \chi + \chi[(A_i \cdot \boldsymbol{\sigma}), \sigma_z]. \qquad (2)$$

That is, A_i^z transforms as electromagnetic vector potential $(\delta A_i^z = \hbar \partial_i \chi)$, while $\mathbf{A}_i^{\parallel} = (A_i^x, A_i^y)$ rotates around $\hat{z}$ by angle 2χ. This observation will prove useful below.

Next, we split the bispinor Ψ into two spin-$\frac{1}{2}$ components, for states at energies near $\pm \Delta$, respectively—and thus take the 4×4 ('Dirac') Hamiltonian (1) to its 2×2 ("Pauli-Schrödinger") low-energy limit [25,26]. Here, we focus on the conduction band (energies E near $+\Delta$) and, to first order in $\frac{E - \Delta}{\Delta} \ll 1$, find the effective-mass Hamiltonian $\mathcal{H}_{\mathbf{p}_0}$ near $\mathbf{p}_0$, with $\bar{\varepsilon}_{\mathbf{p}_0+\mathbf{Q}}(\hat{\mathbf{p}}) \equiv \sigma_z \varepsilon_{\mathbf{p}_0+\mathbf{Q}}(\hat{\mathbf{p}}) \sigma_z$:

$$\mathcal{H}_{\mathbf{p}_0} = \frac{\varepsilon_{\mathbf{p}_0}(\hat{\mathbf{p}}) + \bar{\varepsilon}_{\mathbf{p}_0+\mathbf{Q}}(\hat{\mathbf{p}})}{2} + \frac{[\varepsilon_{\mathbf{p}_0}(\hat{\mathbf{p}}) - \bar{\varepsilon}_{\mathbf{p}_0+\mathbf{Q}}(\hat{\mathbf{p}})]^2}{8\Delta}. \qquad (3)$$

The explicit form of Hamiltonian (3) depends on that of $\varepsilon_{\mathbf{p}_0}(\hat{\mathbf{p}})$ and $\varepsilon_{\mathbf{p}_0+\mathbf{Q}}(\hat{\mathbf{p}})$, in its turn defined by the symmetry of momenta $\mathbf{p}_0$ and $\mathbf{p}_0 + \mathbf{Q}$ in the BZ. Hereafter we focus on the extrema at midpoints Σ of the magnetic Brillouin zone (MBZ) boundary in Fig. 1. At point Σ, the momentum expansion of $\varepsilon_{\mathbf{p}_0}(\hat{\mathbf{p}})$ and $\varepsilon_{\mathbf{p}_0+\mathbf{Q}}(\hat{\mathbf{p}})$ begins with $\pm \mathbf{v} \cdot \hat{\mathbf{p}} + \hat{p}_i^2/2m_i$, with the paramagnetic-state Fermi velocity $\mathbf{v}$ at Σ pointing along the local p_y in Fig. 1, and $m_i = m_x, m_y$ the paramagnetic-state effective masses along and normal to the MBZ boundary. Truncating the momentum expansion of Eq. (3) at quadratic
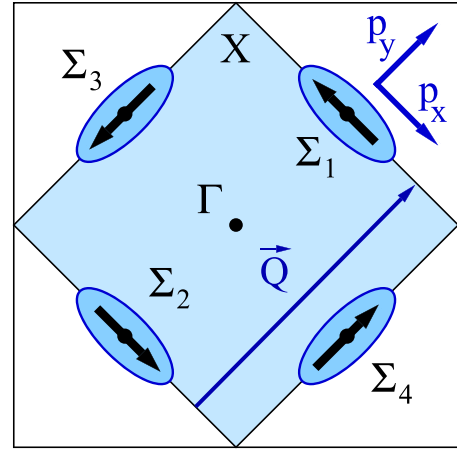

FIG. 1. The Brillouin zone (BZ) of a square-lattice Néel antiferromagnet with wave vector $\vec{\mathbf{Q}} = (\pm \frac{\pi}{a}, \pm \frac{\pi}{a})$. The large square shows the BZ in the paramagnetic state, the shaded square depicts the Brillouin zone in the Néel state (MBZ). The band extrema are assumed to lie at face centers Σ_1-Σ_4 of the MBZ. The p_x, p_y are the local momentum axes near Σ_1, as used in the main text. The ellipses sketch the equal-$E_{\mathbf{p}}$ lines near Σ_1-Σ_4. The bold arrows centered at Σ_1-Σ_4 show the electron spin polarization of low-energy conduction-band bound states in each valley, for a large BP skyrmion of Néel type (see main text).

terms [27], we find

$$\mathcal{H}_{\Sigma} = \frac{(\hat{p}_i + A_i^z \sigma_z)^2}{2m_i^*} + \frac{(A_i^{\parallel})^2}{2m_i} + v(\mathbf{A}_y^{\parallel} \cdot \boldsymbol{\sigma}). \qquad (4)$$

Hamiltonian (4) *is* gauge-invariant: as per Eq. (2), the A_i^z in the kinetic energy transforms as electromagnetic vector potential, while $\mathbf{A}_i^{\parallel} = (A_i^x, A_i^y)$ in the remaining terms transforms by rotation around $\hat{z}$. Moreover, the terms above are the only ones allowed by symmetry to second order in momentum, keeping in mind symmetry under reflection $x \to -x$ [28]. The astute reader will also notice that the second term in Hamiltonian (4) is small relative to the third one as long as the characteristic length scale of the texture remains large compared with the lattice spacing, that is as long as the continuum description of the texture applies. The concrete problem we treat in Sec. III confirms this observation.

The nonuniformity of a texture appears in Hamiltonian (4) via the vector potential $(A \cdot \boldsymbol{\sigma})$ that couples the electron spin to its orbital motion. However, obeying different gauge transformation rules as per Eq. (2), the z-component $A_i^z \sigma_z$ and the "in-plane" spin components $(\mathbf{A}_y^{\parallel} \cdot \boldsymbol{\sigma})$ produce spin-orbit coupling differently: The former induces "gauge" spin-orbit coupling via the Peierls substitution in the kinetic energy, while $v(\mathbf{A}_y^{\parallel} \cdot \boldsymbol{\sigma})$ acts as a texture-induced Zeeman field. In Sec. IV, we will discuss the peculiarities of this spin-orbit coupling in relation to the work [18] of Pekar and Rashba.

Finally, note that m_y^* in Eq. (4) is renormalized relative to m_y in the expansion of $\varepsilon_{\mathbf{p}_0}(\hat{\mathbf{p}})$ and $\varepsilon_{\mathbf{p}_0+\mathbf{Q}}(\hat{\mathbf{p}})$, as per $(m_y^*)^{-1} = (m_y)^{-1} + \frac{v^2}{\Delta}$. Therefore m_y^* is small against m_y: $\frac{m_y^*}{m_y} \sim \frac{\Delta}{\epsilon_F} \ll 1$, while $m_x^* = m_x$ is of the order of band electron mass m or greater [29]. Such a mass anisotropy arises for *any* (not only Néel) $(\frac{\pi}{a}, \frac{\pi}{a})$ order with a gap $\Delta \ll \epsilon_F \equiv m_y v^2$.

Electron-doped cuprates at low-to-optimal doping provide a prominent example [30–32], even if the nature of their ordering remains controversial, with experimental evidence presented both against [33–36] and for [37–42] the presence of (quasi)static Néel order.

III. A TRACTABLE EXAMPLE: BELAVIN-POLYAKOV SKYRMION

Having obtained Hamiltonian (4), let us turn to a concrete problem: the $(\mathbf{A} \cdot \boldsymbol{\sigma})$ defined by a single skyrmion. Consider a centrosymmetric isotropic antiferromagnet with stiffness J and continuum-limit energy density $J(\nabla \hat{\mathbf{n}}_\mathbf{r})^2$. In the topological sector with winding number $\mathcal{Q} = 0, \pm 1, \pm 2, \dots$, the lowest-energy solution is the Belavin-Polyakov (BP) skyrmion [20,21] defined by a single length scale: the radius R. The energy $4\pi J|\mathcal{Q}|$ of the BP skyrmion is independent of R by virtue of scale invariance of energy $J \int d^2\mathbf{r}(\nabla \hat{\mathbf{n}}_\mathbf{r})^2$. Being defined by a single length scale makes the BP skyrmion the simplest case to analyze, which leads us to study Hamiltonian (4) for a $\mathcal{Q} = 1$ BP skyrmion. We focus on a configuration $\hat{\mathbf{n}}_\mathbf{r} = (\sin\theta\cos\phi, \sin\theta\sin\phi, \cos\theta)$ with the polar angle θ depending only on the distance $r = \sqrt{x^2 + y^2}$ to the skyrmion center, and $\phi = \arctan\frac{y}{x}$ being the azimuthal angle in the (x, y) plane. The energy density $J(\nabla \hat{\mathbf{n}}_\mathbf{r})^2$ of such a configuration is invariant under shifting ϕ by a constant γ, usually called "helicity" [10]. Moreover, for the BP skyrmion, the helicity drops out of the electron problem up to the direction of the resulting spin polarization. This allows us to reduce the setting to the $\gamma = 0$ pattern above, commonly called the "Néel" skyrmion.

Note that the latter has its own localized eigenexcitations [43], which, generally, shall be treated on an equal footing with the electron degrees of freedom. However, for a sufficiently small single-ion anisotropy and a not too large BP skyrmion, the proper skyrmion frequencies are small against those of electron motion (see Appendix A). In this limit, treating the electron problem as if the skyrmion were perfectly static is a reasonable first approximation that we now focus on.

To proceed, we need to fix the gauge, that is to select a concrete $U_\mathbf{r}$. We do so by choosing

$$U_\mathbf{r} = (\mathbf{m}_\mathbf{r} \cdot \boldsymbol{\sigma}), \tag{5}$$

with unit vector $\mathbf{m}_\mathbf{r}$ pointing along the bisector between $\hat{z}$ and $\boldsymbol{\Delta}_\mathbf{r}$. Being equivalent to π rotation around $\mathbf{m}_\mathbf{r}$, such a $U_\mathbf{r}$ brings $\boldsymbol{\Delta}_\mathbf{r}$ to point along $\hat{z}$ [12].

The $\mathcal{Q} = 1$ BP skyrmion profile is $\sin\theta = \frac{2z}{1+z^2}$ with $z = \frac{r}{R}$ [20,21] (in passing, notice that $\theta[R] = \frac{\pi}{2}$). In the chosen gauge, calculation of spin-z components A_i^z in the first term of Eq. (4) yields

$$A_x^z = \frac{-\hbar y}{R^2 + r^2}, \quad A_y^z = \frac{\hbar x}{R^2 + r^2}. \tag{6}$$

Thus the skyrmion produces geometric flux $\pm 2\pi\hbar$ for the spin-up and spin-down components of the wave function: $\oint A_i^z dl_i = 2\pi\hbar$, with the integral taken along a large contour of radius $r \gg R$ [44]. Such a flux induces topological spin Hall effect [45–47].

The last term in Hamiltonian (4) takes the form

$$v(\mathbf{A}_y^\parallel \cdot \boldsymbol{\sigma}) = -\frac{\hbar v}{R}\frac{\sigma_x}{1 + z^2} = -\Delta\frac{\xi}{R}\frac{\sigma_x}{1 + z^2}, \tag{7}$$

where, by analogy with superconductivity, we choose to call $\xi = \hbar v/\Delta$ the antiferromagnetic coherence length. This term couples the electron spin to its orbital motion and produces an attractive potential for the spin-up component of the wave function along the $\hat{x}$ axis [48].

Finally, the second term in Eq. (4) creates a repulsive potential

$$\frac{(A_i^\parallel)^2}{2m_i} = \frac{\hbar^2}{2R^2}\left[\frac{1}{m_x} + \frac{1}{m_y}\right]\frac{1}{(1 + z^2)^2}. \tag{8}$$

Comparing the terms (8) and (7), we see that the latter is an $a/R \ll 1$ fraction of the former. That is, the repulsion (8) is negligible relative to the spin-orbit term (7) as long as the continuum description of the skyrmion is valid.

The term (7) is precisely the "texture-induced Zeeman" part of the spin-orbit coupling that we discussed below Eq. (4). Direct inspection shows that, for a large $(R \gg \xi)$ skyrmion, the right-hand side (r.h.s.) of Eq. (7) overwhelms all the other terms with A_i^α in Eq. (4) [49], and creates nondegenerate skyrmion-electron bound states, a key result of our work. At $R \gg \xi$, the low-lying bound states are shallow and spin-polarized in each of the four Σ valleys as shown in Fig. 1 [50].

Note that this polarization is opposite to the one expected from Eq. (7). This is a result of undoing the transformation $U_\mathbf{r}$ of Eq. (5) to restore the original spin axes. While $U_\mathbf{r}$ is substantially nonuniform, the reader will see that, for $R \gg \xi$, it does remain nearly constant over the spatial extent of the low-lying bound states: $U_\mathbf{r} = (\mathbf{m}_\mathbf{r} \cdot \boldsymbol{\sigma}) \approx \sigma_z$. That is, for low-lying bound states, undoing the $U_\mathbf{r}$ amounts to a spin rotation by π around $\hat{z}$, which simply inverts the spin polarization relative to the one dictated by Eq. (7). Notice that for smaller skyrmions low-lying bound states are no longer uniformly spin-polarized: instead, their spinor structure varies substantially over the wave function range.

The mass anisotropy $\frac{m_y^*}{m_x^*} \sim \frac{\Delta}{\epsilon_F} \ll 1$ of Hamiltonian (4) makes the y coordinate "fast" relative to x, and the energies of low-lying bound states can be readily evaluated in the Born-Oppenheimer approximation [51]. For $R \gg \xi$, the energies ϵ_n^c of the bound states generated by the conduction band and labeled by quantum number n can be evaluated by expanding the r.h.s. of Eq. (7) to first order in z^2 and finding the spectrum of the ensuing harmonic oscillator with respect to y:

$$\epsilon_n^c(R) \approx -\Delta\frac{\xi}{R}\left[1 - \sqrt{\frac{2\xi}{R}}\left(n + \frac{1}{2}\right)\right]. \tag{9}$$

Subsequent account of the "slow" coordinate x generates energy levels that we label with quantum number k, with the effective oscillator frequency of the order of $\sqrt{\frac{m_y}{m_x}\frac{a}{\xi}} \ll 1$ relative to the one above:

$$\epsilon_{nk}^c(R) \approx -\Delta\frac{\xi}{R}\left[1 - \sqrt{\frac{2\xi}{R}}\left\{\left(n + \frac{1}{2}\right) + \sqrt{\frac{m_y}{m_x}\frac{a}{\xi}}\left(k + \frac{1}{2}\right)\right\}\right]. \tag{10}$$
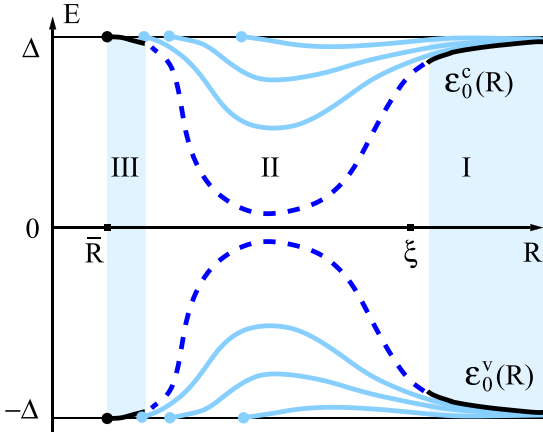
FIG. 2. Energy $\epsilon_0^c(R)$ of BP skyrmion-electron bound state, generated by the conduction band, and of its valence-band counterpart $\epsilon_0^v(R)$ (the highest filled state), sketched as a function of the BP skyrmion radius R. In region I ($R \gg \xi = \frac{\hbar v}{\Delta}$), the bound state is described by low-energy Hamiltonian (4). The $\epsilon_0^c(R)$ is given by Eq. (9) and shown by solid line. In region II ($\bar{R} \ll R \lesssim \xi$), the low-energy approximation breaks down, and the bound state (dashed line) must be found from the full Hamiltonian of a kind (1) in the presence of the skyrmion, which goes beyond the scope of this work. In region III (narrow range $R - \bar{R} \ll \bar{R}$), the bound state, shown by solid line, becomes shallow again. Its disappearance at $R = \bar{R}$ can be described by low-energy Hamiltonian (4) (see main text). Pale lines sketch the higher bound states.

Needless to say, this "fine" structure is much more prone to effects of proper eigenexcitations [43] of the skyrmion than the r.h.s. of Eq. (9), see Appendix A.

For $R \gg \xi$, the bound states (9) and (10) are shallow ($|\epsilon_0^c| \ll \Delta$), and the low-energy approximation of Hamiltonians (3) and (4) remains valid. However, with R decreasing, $|\epsilon_0^c|$ grows to attain the order of Δ at $R \sim \xi$, where the low-energy approximation breaks down along with Hamiltonians (3) and (4), as sketched in Fig. 2.

Now we will show that, with R decreasing further below ξ, the bound state becomes shallow again, and vanishes at an $\bar{R} \sim \sqrt{\frac{m_y}{m_x}}\sqrt{\xi a}$. To make this length scale manifest, we eliminate A_y^z from the first term in Eq. (4) by gauge transformation

$$W = e^{i\sigma_z \chi}, \quad \chi(\tilde{x}, \tilde{y}) = \frac{-\tilde{x}}{\sqrt{1+\tilde{x}^2}} \arctan \frac{\tilde{y}}{\sqrt{1+\tilde{x}^2}}, \quad (11)$$

where $\tilde{x} = \frac{x}{R}$ and $\tilde{y} = \frac{y}{R}$. As a result, Hamiltonian (4) takes the form

$$\tilde{\mathcal{H}}_\Sigma = \frac{\hat{p}_y^2}{2m_y^*} + v(\tilde{\mathbf{A}}_y^{\parallel} \cdot \boldsymbol{\sigma}) + \frac{(A_i^{\parallel})^2}{2m_i} + \frac{(\hat{p}_x + \tilde{A}_x^z \sigma_z)^2}{2m_x}, \quad (12)$$

where $\tilde{A}_x^z = A_x^z + \partial_x \chi$, and

$$(\tilde{\mathbf{A}}_y^{\parallel} \cdot \boldsymbol{\sigma}) = A_y^{\parallel}[\sigma_x \cos 2\chi + \sigma_y \sin 2\chi].$$

In terms of the 'fast' coordinate y, Hamiltonian (12) describes a particle in a one-dimensional potential $\mathcal{U}_x(y)$, parametrically dependent on the "slow" variable x, which again invites the Born-Oppenheimer approximation. Comparing the characteristic value $\frac{\hbar v}{R} = \Delta \frac{\xi}{R}$ of the second term in Eq. (12)

with typical kinetic energy $\frac{\hbar^2}{m_y^* R^2} \approx \Delta(\frac{\xi}{R})^2$ of the trapped electron, we see that the former is indeed small against the latter for $R \ll \xi$, the range in question. The effective bound-state energy is thus defined by the integrated potential $u(x) = \int \mathcal{U}_x(y)dy$ [52]. Contribution of the second term in Eq. (12) to $u(x)$ is

$$u_1(x)\sigma_x = -v \int dy(\tilde{\mathbf{A}}_y^{\parallel} \cdot \boldsymbol{\sigma}) = \hbar v \sigma_x \frac{\sin\left(\frac{\pi \tilde{x}}{\sqrt{1+\tilde{x}^2}}\right)}{\tilde{x}}. \quad (13)$$

The third term in Eq. (12) is an $\frac{a}{R} \ll 1$ fraction of the second, thus its contribution to $u(x)$ can be neglected as long as continuum description of the skyrmion applies ($R \gg a$). By contrast,

$$u_2(x) = \frac{1}{2m_x} \int dy(\tilde{A}_x^z)^2, \quad (14)$$

arising from the last term, requires care since $(\tilde{A}_x^z)^2$ remains finite as $y \to \infty$:

$$A^2(x) \equiv \lim_{y \to \infty} (\tilde{A}_x^z)^2 = \frac{\hbar^2}{R^2} \frac{[\pi/2]^2}{(1+\tilde{x}^2)^3},$$

which makes $u_2(x)$ diverge. We remedy this by writing $(\tilde{A}_x^z)^2 = [(\tilde{A}_x^z)^2 - A^2(x)] + A^2(x)$. The term in the square brackets then gives a finite contribution to $u(x)$, which is suppressed relative to $u_1(x)$ by a factor $\frac{m_y}{m_x} \frac{a}{R}$, and hence remains negligible within continuum description ($R \gg a$). The resulting bound-state energy $w_-(x)$ at a given x is thus defined [52] by $u_1(x)$ alone:

$$w_-(x) = -\frac{m_y^*}{2\hbar^2}[u_1(x)]^2 = -\frac{\Delta}{2} \frac{\sin^2\left(\frac{\pi \tilde{x}}{\sqrt{1+\tilde{x}^2}}\right)}{\tilde{x}^2}. \quad (15)$$

It competes with the repulsive contribution of $A^2(x)$:

$$w_+(x) = \frac{A^2(x)}{2m_x} = \frac{\hbar^2}{2m_x R^2} \frac{[\pi/2]^2}{(1+\tilde{x}^2)^3}. \quad (16)$$

As per Eqs. (6) and (11), $\tilde{A}_x^z$ is odd with respect to y, thus the cross-term $\{\hat{p}_x, \tilde{A}_x^z \sigma_z\}/2m_x$ averages out upon integration over y. As a result, upon switching to the dimensionless coordinate $\tilde{x} = \frac{x}{R}$, the Hamiltonian $\tilde{\mathcal{H}}_x$ reads

$$\tilde{\mathcal{H}}_x = \frac{\hbar^2}{2m_x R^2}\left[-\frac{d^2}{d\tilde{x}^2} + \frac{[\pi/2]^2}{(1+\tilde{x}^2)^3}\right] - \frac{\Delta}{2} \frac{\sin^2\left[\frac{\pi \tilde{x}}{\sqrt{1+\tilde{x}^2}}\right]}{\tilde{x}^2}. \quad (17)$$

Taken alone, the last term above is obviously beyond the low-energy approximation. However, with decreasing R, the repulsion grows relative to attraction, and overcomes it at an $\bar{R} \sim \sqrt{\frac{m_y}{m_x}}\sqrt{\xi a} \ll \xi$. Thus Hamiltonian (17) is valid only in a narrow range $R - \bar{R} \ll \bar{R}$, where the bound state becomes shallow to disappear at $R = \bar{R}$. Notice that $\bar{R} \gg a$ as long as the ratio $\frac{m_y}{m_x}$ is not too small ($\frac{m_y}{m_x} \gg \frac{\Delta}{\epsilon_F}$).

Note that neither the bound state becoming shallow in a narrow range near $\bar{R}$ nor its disappearance at $\bar{R}$ rely on the mass anisotropy: the same behavior obtains for a perfectly isotropic mass, where the Hamiltonian can be diagonalized by solving a single equation for the radial wave function.

Described in this section, the bound-state behavior at large and small skyrmion radii has several implications. These are

convenient to illustrate at half-filling, where the total number of states (itinerant plus bound) generated by the valence band in the presence of the skyrmion equals the number of electrons—that is, the number of unit cells in the sample. By particle-hole symmetry, every bound state $\epsilon_\alpha^c(R)$, split off the conduction band, has a valence-band counterpart $\epsilon_\alpha^v(R) = -\epsilon_\alpha^c(R)$, as shown in Fig. 2. Therefore, for any R, the number of negative-energy states equals the number of electrons. Hence, at zero temperature, all the positive-energy states are empty while all the negative-energy states are filled. Last but not least, notice that the negative-energy bound states rise above the top of the valence band, thus *increasing* the energy cost of the skyrmion. Qualitatively, the energy $\epsilon_0^v(R)$ of the highest filled state behaves as sketched in Fig. 2.

IV. DISCUSSION AND CONCLUSIONS

The skyrmion-electron bound states of Sec. III owe their existence to the 'texture-induced Zeeman' part of the spin-orbit coupling, the last term of Hamiltonian (4). Unlike the 'gauge' term, arising from the Peierls substitution in the kinetic energy [12,24], this term has no equivalent in a ferromagnet. At the same time, it hinges on the lower symmetry of Σ points in the Brillouin zone: at the corner points X or at the center point Γ in Fig. 1, such a term is not allowed.

Notice that, in the effective-mass Hamiltonian of Pekar and Rashba, the spin-orbit coupling is linear in momentum (see Eqs. (4) and (5) of Ref. [18]), as is the "gauge" spin-orbit term in Hamiltonian (4). By contrast, the "texture-induced Zeeman" spin-orbit coupling does not involve electron momentum and hence is qualitatively different.

It is instructive to compare the latter term with other known spin-orbit couplings. To gain perspective, recall that the text-book Pauli spin-orbit coupling appears in the Schrödinger Hamiltonian only as a relic of relativity, in second order of the expansion in the inverse speed of light $1/c$ [25]. Remarkably, in antiferromagnets subject to magnetic field, spin-orbit coupling may appear in *first* order in $1/c$, via a substantial momentum dependence of the g-tensor [42,53,54]. In contrast to all of the above, the texture-induced spin-orbit coupling of Eq. (4) does not involve $1/c$, or the fine-structure constant $\alpha = \frac{e^2}{\hbar c} \approx 1/137$, at all. Instead, the energy scale of the 'texture-induced Zeeman' spin-orbit term $v(\mathbf{A}_y^\parallel \cdot \boldsymbol{\sigma}) \sim \hbar v / L$ is defined by the relevant length scale L of the texture and by the Fermi velocity $v \sim Wa/\hbar$, with W the electron bandwidth and a the lattice spacing. For the Belavin-Polyakov skyrmion we analyzed in Sec. III, L is given by the skyrmion radius R. Compared with W, the "texture-induced Zeeman" term is small only in the measure of L being large against a: $v(\mathbf{A}_y^\parallel \cdot \boldsymbol{\sigma}) \sim W \frac{a}{L}$ (recall that continuum description is limited to $L \gg a$). Relative to the gap Δ, the term is small in the measure of L being large against the Néel coherence length $\xi = \frac{\hbar v}{\Delta}$, that is $v(\mathbf{A}_y^\parallel \cdot \boldsymbol{\sigma}) \sim \Delta \frac{\xi}{L}$.

The skyrmion-electron bound states are nondegenerate. Being limited by the gap, their energy scale is given by Δ. In this regard, the texture-induced spin-orbit coupling in Eq. (4) is a real-space analog of large band-splitting effects, discussed for certain types of antiferromagnets [18,55–58].

We have shown that, in a Néel antiferromagnet with certain locations of the electron band extrema, a skyrmion produces

nondegenerate electron bound states. In each Σ valley, low-lying bound states are spin-polarized as shown in Fig. 1. By virtue of charge neutrality, at half-filling the bound states do not produce a charge density modulation. However, doping the half-filled antiferromagnetic insulator by an extra carrier turns the skyrmion into a charged particle. This effect does not rely on the BP profile we used as an illustration, and appears for *any* credible shape such as that of a domain-wall skyrmion.

Finally, a brief comment on how disorder may limit the validity of our results. A crude bound becomes evident upon comparing the energy $\hbar v/R$ of the low-lying bound states with the disorder-induced scattering rate $1/\tau$ of an electron: for a BP skyrmion of radius $R \gg \xi$, the leading term in Eq. (9) is valid as long as the electron mean free path $l = v\tau$ is large compared with R.

Pekar and Rashba showed [18] how a nonuniformity of magnetization couples electron spin to its orbital motion. However, the analysis of the preceding sections involved no magnetization at all—not even locally. The only quantity present was the staggered ($\mathbf{Q} = (\frac{\pi}{a}, \frac{\pi}{a})$) magnetization and its inhomogeneity. Thus Pekar's and Rashba's insight holds beyond their original statement: in a *general* magnetically ordered system, inhomogeneity begets spin-orbit coupling.

Skyrmion-electron bound states are a new arrival in the family of electron states, localized on topological defects such as dislocations [59], vortices in superconductors [60], or solitons in organic materials [61,62]. Becoming charged in the presence of dopant carriers, the skyrmion can be manipulated by electric field, which may open new possibilities for its use in devices. We hope that our results stimulate further work both on fundamental and applied aspects of this phenomenon.

Note added. Finally, we thank G. Baskaran for pointing out to us earlier studies [63,64] that found skyrmion-electron bound states in an exotic spin liquid (see Appendix B).

APPENDIX A: WHEN CAN ONE TREAT THE BELAVIN-POLYAKOV SKYRMION AS STATIC?

For $R \gtrsim \xi$, treating the BP skyrmion profile as static input to the electron problem requires the bound-state level spacing $\hbar \omega_e \sim \Delta (\frac{\xi}{R})^{\frac{3}{2}}$ in Eq. (9) to be large against the energies of high-frequency localized eigenmodes of the skyrmion. These are bound from above by the spin wave gap $\hbar \Omega_0$ of the bulk magnon spectrum [43]. In the relevant limit of small single-ion anisotropy $K \ll J$, the behavior $\hbar \Omega_0 \sim \sqrt{KJ}$ [65,66] translates the condition $\omega_e \gg \Omega_0$ into $\Delta (\frac{\xi}{R})^{3/2} \gg$

$\sqrt{KJ}$, which means that a sufficiently large BP skyrmion can no longer be treated as static. For a weak enough anisotropy, this limits our treatment to radia

$$R \ll \xi \left(\frac{\Delta}{J}\right)^{2/3} \left(\frac{J}{K}\right)^{1/3}. \tag{A1}$$

Inequality (A1) is meaningful only if its r.h.s. is large compared with ξ, that is if

$$\frac{K}{J} \ll \left(\frac{\Delta}{J}\right)^2. \tag{A2}$$

Now, the conditions (A1), (A2) define the possibility of treating the skyrmion as static when dealing with y, the "fast" coordinate of the electron. As per Eq. (10), for the "slow" coordinate, x, the relevant frequency is $\hbar\omega_e^x \sim \Delta\sqrt{\frac{m_y}{m_x}}\sqrt{\frac{a}{\xi}}(\frac{\xi}{R})^{\frac{3}{2}} \ll \hbar\omega_e$. As a result, the condition for treating the skyrmion as static when dealing with x is more stringent than (A1):

$$R \ll \xi \left(\frac{\Delta}{\epsilon_F}\right)^{1/3} \left(\frac{m_y}{m_x}\right)^{1/3} \left(\frac{\Delta}{J}\right)^{2/3} \left(\frac{J}{K}\right)^{1/3}. \tag{A3}$$

Inequality (A3) makes sense only if its r.h.s. is large compared with ξ, that is if

$$\frac{K}{J} \ll \left(\frac{\Delta}{J}\right)^2 \frac{m_y}{m_x} \frac{\Delta}{\epsilon_F}. \tag{A4}$$

Put otherwise, the levels emerging from quantizing the electron motion along the "slow" coordinate x define the "fine" structure of the bound-state spectrum as opposed to the "gross" structure arising from quantization along the "fast" coordinate y. This fine structure can be treated in the static-skyrmion approximation under conditions (A3), (A4) that are, naturally, much more stringent than similar inequalities (A1), (A2) for the gross structure of Eq. (9). At the same time, no matter how small the ω_e/Ω_0 ratio, a sufficiently large number of skyrmion eigenexcitations would eventually influence the excited electron bound states (at an appropriately high order of perturbation theory).

APPENDIX B: EARLIER WORK [17,63,64,67–69]

In this section of Appendix, we discuss some of the relevant early work.

S. John and A. Golubentsev [63,64] studied the Hubbard model on a square lattice in a topological spin liquid state, defined by two key properties: (i) checkerboard Néel order, and (ii) antiperiodicity of the electron wave function along closed path around any elementary plaquette of the lattice. As a consequence, the unit cell in such a state quadruples relative to the underlying square lattice, and the electron wave function is thus a 4-spinor. The model band extrema fall at the very same points $\Sigma = (\pm\frac{\pi}{a}, \pm\frac{\pi}{a})$ that we focused on, and all the four points Σ are equivalent in the "ordered" Brillouin zone. The resulting "Dirac" electron spectrum near Σ is thus isotropic by symmetry.

As opposed to the above, in the Néel state of our interest the unit cell doubles rather than quadruples and, therefore, the

electron wave function is a bispinor rather than a 4-spinor. Contrary to being all equivalent in the spin liquid state, in the Néel phase the four points Σ split into two inequivalent pairs $\Sigma_{1,2}$ and $\Sigma_{3,4}$, shown in Fig. 1. In contrast to the spin-liquid state, the symmetry of the Néel state does not require the electron spectrum near the Σ points to be isotropic. Quite to the contrary, it tends to be strongly anisotropic, consistently with experimental findings [30–32] in a number of cuprates.

Lastly, the skyrmion-electron bound states we found are nondegenerate. In each of the four Σ valleys, low-lying bound states are spin-polarized as shown in Fig. 1, whereas the bound states of Refs. [63,64] are doubly degenerate as a consequence of the elevated symmetry of the spin-liquid state.

To summarize, the similarities between the skyrmion-electron bound states of our work and those found by John and Golubentsev arise from Néel order being an ingredient of the spin liquid studied in Refs. [63,64]. Such similarities include the shallow character of bound states at large BP skyrmion radia, although John and Golubentsev have not explored the low-energy limit, instead opting for solving their full 8×8 Hamiltonian numerically.

The differences between our results and those of John and Golubentsev stem from the features of their spin liquid that are not inherent to a generic Néel state that we studied, such as (i) an elevated symmetry of the spin liquid and (ii) the wave function antiperiodicity under translation around any elementary plaquette of the square lattice. Such differences lead to double degeneracy of the bound states found by John and Golubentsev, while ours are nondegenerate.

Now we turn to the work [17] by R. Cheng and Q. Niu, who derived coupled quasiclassical equations of motion for the electron momentum, coordinate and spin in an antiferromagnetic texture. By construction, such a description holds only for large quantum numbers and, in fact, the equations of Cheng and Niu become singular at the MBZ boundary ($\xi \to 0$), see the r.h.s. of Eq. (8c) of Ref. [17]. By contrast, our effective electron Hamiltonian (3-4) covers both the quasiclassical regime and the extreme quantum limit as long as the electron energies are close to the gap edge ($\frac{|E-\Delta|}{\Delta} \ll 1$).

Finally, we would like to mention the work [67,68] on different versions of the t-J model of high-temperature superconductivity. These studies were performed on small clusters in the atomic limit, with exchange integrals substantial or even large compared with the hopping matrix elements. The authors of both Refs. [67,68] reach a conclusion that is, in a way, reciprocal to ours ("a skyrmion produces electron bound states"): namely, that introducing a dopant carrier into a single CuO plane renders a skyrmion [67] or a half-skyrmion [68] configuration energetically favorable [69]. When applied to a single dopant carrier bound to a skyrmion, this conclusion stems from neglecting the valence band giving rise to filled bound states, whose energy *increases* rather than decreases (see Fig. 2), and thus overwhelms the energy gain found in Refs. [67,68]. A more technical difference with respect to our work is that the studies [67,68] were performed in the atomic limit, and thus produced skyrmion sizes of the order of the lattice spacing, where the continuum description is not applicable.

[1] K. Becker, M. Becker, and J. H. Schwarz, *String Theory and M-Theory* (Cambridge University Press, Cambridge, 2007).

[2] M. Rho and I. Zahed (eds.), *The Multifaceted skyrmion* (World Scientific, 2016).

[3] C. Back, V. Cros, H. Ebert, K. Everschor-Sitte, A. Fert, M. Garst, T. Ma, S. Mankovsky, T. L. Monchesky, M. Mostovoy *et al.*, J. Phys. D: Appl. Phys. **53**, 363001 (2020).

[4] A. Fert, Rev. Mod. Phys. **80**, 1517 (2008).

[5] P. A. Grünberg, Rev. Mod. Phys. **80**, 1531 (2008).

[6] A. Fert and F. N. V. Dau, C. R. Phys. **20**, 817 (2019).

[7] O. Gomonay, T. Jungwirth, and J. Sinova, Phys. Status Solidi RRL **11**, 1700022 (2017).

[8] V. Baltz, A. Manchon, M. Tsoi, T. Moriyama, T. Ono, and Y. Tserkovnyak, Rev. Mod. Phys. **90**, 015005 (2018).

[9] L. Šmejkal, Yu. Mokrousov, B. Yan, and A. H. MacDonald, Nat. Phys. **14**, 242 (2018).

[10] B. Göbel, I. Mertig, and O. A. Tretiakov, Phys. Rep. **895**, 1 (2021).

[11] T. Jungwirth, X. Marti, P. Wadley, and J. Wunderlich, Nat. Nanotechnol. **11**, 231 (2016).

[12] G. Tatara, H. Kohno, and J. Shibata, Phys. Rep. **468**, 213 (2008).

[13] N. Nagaosa and Y. Tokura, Nat. Nanotechnol. **8**, 899 (2013).

[14] A. H. MacDonald and M. Tsoi, Philos. Trans. R. Soc. A **369**, 3098 (2011).

[15] E. V. Gomonay and V. M. Loktev, Low Temp. Phys. **40**, 17 (2014); Fiz. Nizk. Temp. **40**, 22 (2014).

[16] A. Manchon, J. Železný, I. M. Miron, T. Jungwirth, J. Sinova, A. Thiaville, K. Garello, and P. Gambardella, Rev. Mod. Phys. **91**, 035004 (2019).

[17] R. Cheng and Q. Niu, Phys. Rev. B **86**, 245118 (2012).

[18] S. I. Pekar and E. I. Rashba, Zh. Eksp. Teor. Fiz. **47**, 1927 (1964) [Sov. Phys. JETP **20**, 1295 (1965)].

[19] C. Herring, in *Magnetism*, edited by George T. Rado and Harry Suhl (Academic Press, New York, London, 1966), Vol. IV, Chap. XIII.

[20] A. A. Belavin and A. M. Polyakov, Pis'ma Zh. Eksp. Teor. Fiz. **22**, 503 (1975) [JETP Lett. **22**, 245 (1975)].

[21] R. Rajaraman, *Solitons and Instantons* (North-Holland, Amsterdam, 1989).

[22] N. I. Kulikov and V. V. Tugushev, Usp. Fiz. Nauk **144**, 643 (1984); Sov. Phys. Usp. **27**, 954 (1984).

[23] C. Kittel, *Quantum Theory of Solids* (John Wiley & Sons, Inc., New York – London, 1963).

[24] G. E. Volovik, J. Phys. C: Solid State Phys. **20**, L83 (1987).

[25] V. B. Berestetskǐ, E. M. Lifshitz, and L. P. Pitaevskǐ, Course of Theoretical Physics, Vol. 4, *Quantum Electrodynamics* (Pergamon Press, Oxford, 1982).

[26] L. H. Ryder, *Quantum Field Theory* (Cambridge University Press, Cambridge, 1996).

[27] The terms omitted when passing from Eq. (3) to (4) are higher order in momentum. They are negligible as long as the low-energy approximation of Eqs. (3) and (4) is valid.

[28] Symmetry under reflection $x \to -x$ is imposed by the small group of point Σ, and thus forbids the appearance of gauge-invariant terms such as $(A_x^{\parallel} \cdot A_y^{\parallel})$ and $[A_x^{\parallel} \times A_y^{\parallel}]$.

[29] Notice that, with only the nearest-neighbor hopping, m_x at Σ is infinite.

[30] N. P. Armitage, F. Ronning, D. H. Lu, C. Kim, A. Damascelli, K. M. Shen, D. L. Feng, H. Eisaki, Z.-X. Shen, P. K. Mang *et al.*, Phys. Rev. Lett. **88**, 257001 (2002).

[31] H. Matsui, T. Takahashi, T. Sato, K. Terashima, H. Ding, T. Uefuji, and K. Yamada, Phys. Rev. B **75**, 224514 (2007).

[32] D. Song, G. Han, W. Kyung, J. Seo, S. Cho, B. S. Kim, M. Arita, K. Shimada, H. Namatame, M. Taniguchi *et al.*, Phys. Rev. Lett. **118**, 137001 (2017).

[33] G. M. Luke, L. P. Le, B. J. Sternlieb, Y. J. Uemura, J. H. Brewer, R. Kadono, R. F. Kiefl, S. R. Kreitzman, T. M. Riseman, C. E. Stronach *et al.*, Phys. Rev. B **42**, 7981 (1990).

[34] E. M. Motoyama, G. Yu, I. M. Vishik, O. P. Vajk, P. K. Mang, and M. Greven, Nature **445**, 186 (2007).

[35] P. K. Mang, S. Larochelle, A. Mehta, O. P. Vajk, A. S. Erickson, L. Lu, W. J. L. Buyers, A. F. Marshall, K. Prokes, and M. Greven, Phys. Rev. B **70**, 094507 (2004).

[36] H. Saadaoui, Z. Salman, H. Luetkens, T. Prokscha, A. Suter, W. A. MacFarlane, Y. Jiang, K. Jin, R. L. Greene, E. Morenzoni, and R. F. Kiefl, Nat. Commun. **6**, 6041 (2015).

[37] K. Yamada, K. Kurahashi, T. Uefuji, M. Fujita, S. Park, S.-H. Lee, and Y. Endoh, Phys. Rev. Lett. **90**, 137004 (2003).

[38] H. J. Kang, P. Dai, H. A. Mook, D. N. Argyriou, V. Sikolenko, J. W. Lynn, Y. Kurita, S. Komiya, and Y. Ando, Phys. Rev. B **71**, 214512 (2005).

[39] Y. Dagan, M. C. Barr, W. M. Fisher, R. Beck, T. Dhakal, A. Biswas, and R. L. Greene, Phys. Rev. Lett. **94**, 057005 (2005).

[40] W. Yu, J. S. Higgins, P. Bach, and R. L. Greene, Phys. Rev. B **76**, 020503(R) (2007).

[41] A. Dorantes, A. Alshemi, Z. Huang, A. Erb, T. Helm, and M. V. Kartsovnik, Phys. Rev. B **97**, 054430 (2018).

[42] R. Ramazashvili, P. D. Grigoriev, T. Helm, F. Kollmannsberger, M. Kunz, W. Biberacher, E. Kampert, H. Fujiwara, A. Erb, J. Wosnitza, R. Gross, and M. V. Kartsovnik, npj Quantum Mater. **6**, 11 (2021).

[43] V. P. Kravchuk, O. Gomonay, D. D. Sheka, D. R. Rodrigues, K. Everschor-Sitte, J. Sinova, J. van den Brink, and Yu. Gaididei, Phys. Rev. B **99**, 184429 (2019).

[44] This is true for *any* $\mathcal{Q} = 1$ skyrmion profile. For an arbitrary $\mathcal{Q}$, the corresponding flux is $\pm 2\pi \mathcal{Q}$.

[45] G. Yin, Y. Liu, Y. Barlas, J. Zang, and R. K. Lake, Phys. Rev. B **92**, 024411 (2015).

[46] P. M. Buhl, F. Freimuth, S. Blügel, and Yu. Mokrousov, Phys. Status Solidi RRL **11**, 1700007 (2017).

[47] C. A. Akosa, O. A. Tretiakov, G. Tatara, and A. Manchon, Phys. Rev. Lett. **121**, 097204 (2018).

[48] The strikingly simple r.h.s. of Eq. (7) is a remarkable property of the BP skyrmion.

[49] This conclusion can be reached by direct comparison, with the single exception of the cross-term $V = \{p_y, A_y^z \sigma_z\}/2m_y^*$. For the latter, the presence of σ_z implies that this term has matrix elements only across the gap, and thus its contribution is suppressed by the perturbation-theory factor of the order of $V/\Delta \ll 1$.

[50] For chirality $\gamma \neq 0$, spin polarization of the bound state is tilted by γ relative to the one shown in Fig. 1.

[51] J. C. Tully, Perspective on Zur Quantentheorie der Molekeln, in *Theoretical Chemistry Accounts*, edited by C. J. Cramer and D. G. Truhlar (Springer, Berlin, Heidelberg, 2000).

[52] L. D. Landau and E. M. Lifshitz, Course of Theoretical Physics, Vol. 3, *Quantum Mechanics, Non-relativistic Theory* (Pergamon Press, Oxford, 1991).

[53] R. Ramazashvili, Phys. Rev. Lett. **101**, 137202 (2008).

[54] R. Ramazashvili, Phys. Rev. B **79**, 184432 (2009).

[55] S. Hayami, Y. Yanagi, and H. Kusunose, J. Phys. Soc. Jpn. **88**, 123702 (2019).

[56] L.-D. Yuan, Z. Wang, J.-W. Luo, E. I. Rashba, and A. Zunger, Phys. Rev. B **102**, 014422 (2020).

[57] H. Reichlová, R. L. Seeger, R. González-Hernández, I. Kounta, R. Schlitz, D. Kriegner, P. Ritzinger, M. Lammel, M. Leiviskä, V. Petříček *et al.*, arXiv:2012.15651.

[58] L. Šmejkal, J. Sinova, and T. Jungwirth, Phys. Rev. X **12**, 031042 (2022).

[59] R. Landauer, Phys. Rev. **94**, 1386 (1954).

[60] C. Caroli, P. G. De Gennes, and J. Matricon, Phys. Lett. **9**, 307 (1964).

[61] S. A. Brazovskii and N. N. Kirova, Sov. Sci. Rev. A **5**, 99 (1984).

[62] A. J. Heeger, S. Kivelson, J. R. Schrieffer, and W.-P. Su, Rev. Mod. Phys. **60**, 781 (1988).

[63] S. John and A. Golubentsev, Phys. Rev. Lett. **71**, 3343 (1993).

[64] S. John and A. Golubentsev, Phys. Rev. B **51**, 381 (1995).

[65] C. Kittel, Phys. Rev. **82**, 565 (1951).

[66] S. M. Rezende, A. Azevedo, and R. L. Rodríguez-Suárez, J. Appl. Phys. **126**, 151101 (2019).

[67] S. Haas, F. C. Zhang, F. Mila, and T. M. Rice, Phys. Rev. Lett. **77**, 3021 (1996).

[68] T. Morinari, J. Phys. Soc. Jpn. **81**, 074716 (2012).

[69] Early on, the possibility of a skyrmion appearing around a dopant carrier in a quantum antiferromagnet was pointed out by B. I. Shraiman and E. D. Siggia, Phys. Rev. Lett. **61**, 467 (1988).